Theory of coherent transition radiation generated at a plasma-vacuum interface

C. B. Schroeder, E. Esarey, J. van Tilborg,* and W. P. Leemans

Lawrence Berkeley National Laboratory,

University of California, Berkeley, California 94720

(Dated: June 26, 2003)

Abstract

Transition radiation generated by an electron beam, produced by a laser wakefield accelerator operating in the self-modulated regime, crossing the plasma-vacuum boundary is considered. The angular distributions and spectra are calculated for both the incoherent and coherent radiation. The effects of the longitudinal and transverse momentum distributions on the differential energy spectra are examined. Diffraction radiation from the finite transverse extent of the plasma is considered and shown to strongly modify the spectra and energy radiated for long wavelength radiation. This method of transition radiation generation has the capability of producing high peak power THz radiation, of order 100 μJ/pulse at the plasma-vacuum interface, which is several orders of magnitude beyond current state-of-the-art THz sources.

PACS numbers: 41.60.-m, 52.38.Kd

*Also at Technische Universiteit Eindhoven, the Netherlands.

I. INTRODUCTION

Radiation in the THz and far infrared frequency regimes is used in many areas of research including biological imaging, material screening, semi-conductor imaging, surface chemistry and high-field condensed matter studies [1–3]. Laser-based THz sources have been developed that rely on switched photo-conducting antennas ([4] and references therein) or optical rectification of femtosecond pulse trains [5]. Since the radiation emission is either triggered by or directly produced from a laser, the THz radiation and laser pulses are intrinsically synchronized thereby enabling pump-probe experiments. Large aperture biased GaAs structures, operated at 1 kHz repetition rate, have produced on the order of 0.5 μJ/pulse [6]. Most other sources that use lasers have operated at high frequency (10's of MHz) with μW–mW level average power (i.e., 10's of fJ–nJ per pulse). Increasing the peak power and average power of THz and far infrared sources would benefit numerous applications, such as rapid two-dimensional imaging [3] and high-field studies that require multi-MV/cm fields [2].

Relativistic electron beams can also be used to produce THz and long wavelength radiation through a variety of mechanisms that include synchrotron radiation (e.g., emitted when an electron trajectory is bent in a magnetic field), transition radiation (emitted when an electron traverses a medium with spatially varying dielectric properties, e.g., when an electron propagates through a metallic foil) or diffraction radiation (e.g., emitted when an electron propagates through an aperture) [7]. Radiation emitted by these mechanisms will be coherent when the bunch length (or any longitudinal structure on the bunch) is shorter than the wavelength of interest. The radiated power then scales quadratically with the total charge, rather than linear as in the case of incoherent emission. Coherent radiation can be many orders of magnitude brighter than incoherent radiation since typical electron bunches contain between 10^7 to 10^{10} electrons per bunch. For example, production of coherent high average power THz synchrotron radiation peaking at approximately 0.6 THz has been demonstrated using 40 MeV, 500 fs duration electron bunches with pC charge levels produced by a high repetition rate (37 MHz) linear accelerator [8]. Although such a high average power source will have a wide variety of applications, the amount of energy per pulse was comparable to state-of-the-art solid state based THz sources ($< 1\mu$J/pulse) and does not benefit from intrinsic synchronization with an external laser, which is desired for pump-probe experiments.

Recently, researchers at Lawrence Berkeley National Laboratory (LBNL) have demonstrated a laser-based source of THz radiation that relies on the coherent transition radiation produced by a dense relativistic electron bunch traversing a plasma-vacuum interface [9]. In these experiments, a 10 TW, 50 fs laser pulse interacting with a gas jet was used to generate self-trapped electron bunches via the mechanism of a laser wakefield accelerator (LWFA) in the self-modulated regime [10]. The energy per THz pulse in these experiments was limited by the narrow transverse dimension of the plasma to $\sim$ 5 nJ within a 30 mrad collection angle and was observed to scale quadratically with bunch charge, consistent with coherent emission. The analysis presented below indicates that $\sim$ 1 μJ/pulse is produced within a 100 mrad angle and that optimization of this table-top source could provide 100 μJ/pulse. Together with intrinsic synchronization to a laser pulse, this allows numerous applications in THz imaging and nonlinear ultrafast science.

This laser-plasma source of THz radiation benefits from the extremely dense and ultrashort electron bunches generated using a LWFA (for a review of laser-plasma-based accelerators, see Ref. [11]). The electron bunches produced by this ultra-intense laser-plasma interaction have been characterized experimentally [10, 12–17] and using numerical simulations [18–20]. The self-modulated LWFA produces multi-nC electron bunches of duration on the order of the laser pulse length ($\lesssim$ 100 fs), radius on the order of the laser spot size ($\sim$ 5 μm), and with a longitudinal momentum distribution that is well-modeled by a Boltzmann distribution, typically with a temperature of a few MeV. Inside the plasma, background ions provide space charge shielding that prevent blow-up of the dense electron bunches. After exiting the plasma, space charge and energy spread effects cause bunch density reduction through bunch lengthening and transverse expansion [21]. Therefore, to produce high peak power coherent radiation, emission must occur before propagation in vacuum. This occurs naturally in a self-modulated LWFA by relying on the coherent transition radiation produced by the ultrashort, dense electron bunch at the plasma-vacuum boundary.

The theory of transition radiation by a single electron, first studied by Ginzburg and Frank [22], is extensively treated in the monograph by Ter-Mikaelian [23]. The passage of a charged particle through a spatially-inhomogeneous media results in a transient polarization of the dielectric, and radiation is emitted by the transient polarization current. Coherent transition radiation has been observed and used to diagnose the electron beam properties by passing the electron beam through a metallic foil (for example, see Refs. [24–28]). Recently,

Zheng *et al.* [29] discussed the spectrum of transition radiation in the optical region due to a hot electron beam with structure at half the laser wavelength generated by a laser-matter interaction.

In this paper, properties of incoherent and coherent transition radiation are analyzed for parameter regimes relevant to the production of THz radiation at a plasma-vacuum boundary by electron bunches from a self-modulated LWFA. Included are the effects of a large spread in longitudinal momentum, the effects of the transverse beam momentum (i.e., beam emittance), and the effects of the finite transverse size of the plasma. In the long-wavelength regime characteristic of THz radiation, the transverse extent of the self-fields of the electrons, which is of the order $\sim \lambda\gamma$, can be comparable to the transverse dimensions of the plasma. Here λ is the radiation wavelength and γ is the relativistic Lorentz factor. In this regime, the finite transverse boundary of a dielectric will produce coherent diffraction radiation [30]. The coherent diffraction radiation from the finite transverse size of the plasma will strongly modify the radiation energy spectra and suppress the generation of long wavelength transition radiation.

This paper is organized as follows. The basic description and scalings of transition radiation are presented in Sec. II. In Sec. III, a detailed calculation of the energy radiated by a non-evolving electron bunch traversing a dielectric-vacuum interface is presented. Section IV considers the incoherent transition radiation (ITR) of an electron bunch including the effects of the electron beam longitudinal and transverse momentum distributions. Section V considers coherent transition radiation (CTR). Section VI discusses the effect of diffraction radiation due to the finite transverse size of the plasma-vacuum boundary. In Sec. VII we present an example of the coherent radiation produced by a self-modulated LWFA generated electron bunch. A summary and discussion is presented in Sec. VIII.

II. BASIC DESCRIPTION AND SCALINGS OF TRANSITION RADIATION

To illustrate the potential of CTR generated at the plasma-vacuum boundary as a radiation source, a simplified, idealized description is presented in this section that uses the standard description of transition radiation (for example, see Ref. [31], p. 190) for electrons transiting a metallic foil into vacuum. For radiation wavelengths of interest (e.g., $\lambda \sim 500$ μm or radiation frequency $\omega \sim 4 \times 10^{12}$ s^{-1}), the plasma for typical densities (e.g.,

plasma number density $n \sim 10^{19}$ cm^{-3} or electron plasma frequency $\omega_p \sim 2 \times 10^{14}$ s^{-1}) is highly overdense, i.e., $\omega_p^2 \gg \omega^2$. Furthermore, since the scale length of the plasma-vacuum boundary is small compared to a radiation formation length (the radiation formation length scales as $\sim \gamma^2\lambda$), the plasma-vacuum interface can be approximated as a step function. Hence, the formulae describing transition radiation in the limit of a metallic foil in vacuum are a good approximation, provided the plasma can be modeled as semi-infinite. These approximations and assumptions will be discussed in more detail in the following sections.

Consider a single energetic electron emerging from a high density ($\omega_p^2 \gg \omega^2$), semi-infinite plasma into vacuum (step transition), traveling normal to the plasma surface. The energy radiated from a single electron per unit frequency $d\omega$, per unit solid angle $d\Omega$ is given by

$$\frac{d^2W_e}{d\omega d\Omega} = \frac{r_e m_e c}{\pi^2} \frac{\beta^2 \sin^2\theta}{(1-\beta^2\cos^2\theta)^2} \ , \tag{1}$$

where θ is the observation angle with respect to the electron trajectory (assumed to be normal to the plasma surface), β is the electron velocity normalized to the speed of light c, m_e is the electron rest mass, and r_e is the classical electron radius. The radiation pattern is zero along the axis ($\theta = 0$) and peaks at a radiation cone angle of $\theta \sim 1/\gamma$ (assuming $\gamma \gg 1$). Notice that the differential energy spectrum $d^2W_e/d\omega d\Omega$ is independent of frequency. In practice, however, the maximum wavelength radiated will be limited, for example, by the physical dimensions of the system, as will be discussed in Sec. VI, whereas the minium wavelength radiated will be limited, for the case of CTR, by the electron bunch dimensions. Integrating over all angles yields

$$\frac{dW_e}{d\omega} = \frac{r_e m_e c}{2\pi\beta} \left[(1+\beta^2) \ln\left(\frac{1+\beta}{1-\beta}\right) - 2\beta \right] \ , \tag{2}$$

which, in the highly-relativistic limit $\gamma \gg 1$, reduces to $dW_e/d\omega \simeq (2/\pi) r_e m_e c \ln\gamma$.

Consider now the energy radiated by a monoenergetic electron bunch in the limit of zero emittance and beam radius. For wavelengths short compared to the bunch length, the radiation from the electrons sums incoherently, i.e., $W_{\rm ITR} \simeq N W_e$, where N is the number of electrons in the bunch. For wavelengths long compared to the bunch length, the radiation sums coherently, i.e., $W_{\rm CTR} \simeq N^2 W_e$. In particular, the total coherent radiated energy over all angles and frequencies is given by

$$W_{\rm tot} \simeq \left(4 r_e m_e c^2\right) N^2 (\ln\gamma)/\lambda_{\rm min} \ , \tag{3}$$

assuming $\gamma \gg 1$, where $\lambda_{\rm min}$ is the minimum wavelength for which the bunch radiates coherently and is determined by the electron bunch dimensions, as will be discussed more rigorously in the following sections. The energy radiated into a narrow frequency band $\Delta\omega$ about the frequency $\omega = 2\pi c/\lambda < 2\pi c/\lambda_{\rm min}$ is given approximately by multiplying the above equation by the quantity $(\lambda_{\rm min}/\lambda)(\Delta\omega/\omega)$. Equation (3) can be written in practical units as $W_{\rm tot}[{\rm J}] \simeq 3.6 \times 10^{-2} (Q[{\rm nC}])^2 (\ln\gamma)/\lambda_{\rm min}[\mu{\rm m}]$, where Q is the bunch charge. For example, Q = 5 nC ($N = 3.1 \times 10^{10}$), $\gamma = 10$, and $\lambda_{\rm min} = 200$ μm give $W_{\rm tot} \simeq 10$ mJ, which is several orders of magnitude beyond that of conventional sources.

Owing to the N^2 scaling of CTR, the total radiated energy can approach the total kinetic energy of the bunch $W_b = N m_e c^2 (\gamma - 1)$ for electron bunches with sufficiently high charge (large N) and low energy (small γ). The above expressions hold only if the energy radiated is small compared to the bunch kinetic energy. Requiring $W_{\rm tot} < W_b$ implies $N < 0.25 (\lambda_{\rm min}/r_e)(\gamma/\ln\gamma)$. For example, $\gamma = 10$, $\lambda_{\rm min} = 200$ μm implies $N < 7.7 \times 10^{10}$ (12 nC).

The above expressions indicate that electron energy loss via CTR can be a significant factor in determining the final electron energy spectra emerging from a LWFA. In particular, in the self-modulated regime, experiments have measured multiple-nC bunches (up to 10 nC observed in experiments at LBNL), with the bulk of electrons occurring at low energies, i.e., the energy distribution falls off exponentially with a temperature of a few MeV [32]. Furthermore, the electron bunch length in the plasma is expected to be on the order of the laser pulse duration, i.e., < 100 fs. This implies that CTR could be emitted with wavelengths on the order of $\lambda \gtrsim 30$ μm. The above expressions indicate that the energy radiated by CTR can be on the order of the kinetic energy of the bunch, particularly for short, low energy bunches of high charge. Hence, as such bunches emerge from the plasma, the CTR emitted at the plasma-vacuum interface can significantly modify the electron energy spectra by shifting the spectra to lower energies. A self-consistent description of this problem (e.g., by including electron recoil) is beyond the scope of this paper. In the following, sufficiently low bunch charge and sufficiently long bunch lengths will be assumed such that the electron energy can be assumed unperturbed as it crosses the plasma-vacuum boundary.

Another quantity of interest to experiments is the energy radiated into a small cone about

the propagation axis. Expanding Eq. (1) for small angles $\theta^2 \ll 1$ gives

$$\frac{d^2W_e}{d\omega d\Omega} \simeq \frac{r_e m_e c}{\pi^2} \frac{\beta^2\gamma^4\theta^2}{(1+\beta^2\gamma^2\theta^2)^2} \,. \tag{4}$$

Integrating over the solid angle from $0 \le \theta \le \theta_0 \ll 1$ yields

$$\frac{dW_e}{d\omega} \simeq \frac{r_e m_e c}{\pi\beta^2} \left[\ln(1+\beta^2\gamma^2\theta_0^2) - \frac{\beta^2\gamma^2\theta_0^2}{1+\beta^2\gamma^2\theta_0^2} \right] \,, \tag{5}$$

which in the limit $\beta^2\gamma^2\theta_0^2 \ll 1$, i.e., small angles compared to the cone angle of maximum emission $1/(\beta\gamma)$, gives

$$\frac{dW_e}{d\omega} \simeq \frac{r_e m_e c}{2\pi} \beta^2\gamma^4\theta_0^4 \,. \tag{6}$$

Hence, the total CTR energy radiated into a narrow frequency band $\Delta\omega$ about the frequency $\omega = 2\pi c/\lambda < 2\pi c/\lambda_{\rm min}$ by a monoenergetic bunch is given approximately by

$$W_{\rm tot} \simeq N^2 \frac{r_e m_e c^2}{\lambda} \beta^2\gamma^4\theta_0^4 \frac{\Delta\omega}{\omega} \tag{7}$$

or $W_{\rm tot}[{\rm mJ}] \simeq 9.0(Q[{\rm nC}])^2(\gamma\theta_0)^4(\Delta\omega/\omega)/\lambda[\mu{\rm m}]$, assuming $\gamma^2 \gg 1$. For example, $Q = 5$ nC ($N = 3.1 \times 10^{10}$), $\gamma = 10$, $\lambda_{\rm min} = 200$ μm, and $\theta_0 = 10$ mrad give $W_{\rm tot} \simeq 0.11(\Delta\omega/\omega)$ μJ. Due to the strong dependence on electron energy and angle, $W_{\rm tot} \propto (\gamma\theta_0)^4$, the measured energy can easily be increased by increasing either the electron energy γ or the cone angle θ_0 of the collection optics.

The above results apply to an idealized case of a short monoenergetic bunch in the limit of zero emittance and zero radius interacting with a semi-infinite plasma slab. In the following sections, non-ideal effects will be accounted for in the calculation of the radiation spectrum, including energy spread, emittance, finite bunch size, and the finite transverse size of the plasma.

III. GENERAL FORMALISM AND ASSUMPTIONS

In this section, we derive the total energy radiated by an electron bunch, with arbitrary spatial and momentum distributions, crossing a plasma-vacuum interface. We will consider a dielectric (plasma-vacuum) interface in the (x, y) plane such that there is plasma for $z < 0$ and vacuum for $z > 0$. The approximation of a step transition from plasma to vacuum will be valid for provided the transition from plasma to vacuum is much less than the formation

length [33] of the radiation $L_f \simeq \lambda/(\gamma^{-2}+\theta^2)$. We will also consider an electron beam current that has the form

$$\boldsymbol{J}_{\rm b}(\boldsymbol{x},t) = -e\sum_{j=1}^{N} c\boldsymbol{\beta}_j \delta\left(\boldsymbol{x}-\boldsymbol{r}_j - c\boldsymbol{\beta}_j t\right) \ , \tag{8}$$

where N is the number of electrons in the bunch, e is the electronic charge, c is the speed of light in vacuo, and $\boldsymbol{r}_j$ is the position of the $j^{\rm th}$ electron with velocity $\boldsymbol{v}_j = c\boldsymbol{\beta}_j$. The geometry of the calculation is shown in Fig. 1. The dielectric interface lies at $z=0$ in the (x,y) plane. Each ($j^{\rm th}$) electron in the bunch traverses the plasma-vacuum interface with velocity $\boldsymbol{v}_j = c\boldsymbol{\beta}_j = c(\beta_{xj},\beta_{yj},\beta_{zj}) = c\beta_j(\sin\psi_j\cos\varphi_j, \sin\psi_j\sin\varphi_j, \cos\psi_j)$. Without loss of generality we may assume that the observation vector $\boldsymbol{R}$ (or radiation wavenumber vector $\boldsymbol{k}$) is in the (x,z) plane, where θ is the angle between the observation vector and the z axis. We will assume that $|\boldsymbol{r}_{\perp j}(z=0)| \ll R\sin\theta$ for each electron, such that the beam-boundary interaction may be treated as a point source at the observation position $\boldsymbol{R}$.

A. Radiation field

The Maxwell equations can be combined and written as the following wave equation [7]

$$\left(c^2\nabla^2 - \partial_t^2\right)\boldsymbol{E} = 4\pi\partial_t\left(\boldsymbol{J}_{\rm b}+\boldsymbol{J}_{\rm p}\right) + 4\pi c^2\nabla\left(\rho_{\rm b}+\rho_{\rm p}\right) \ , \tag{9}$$

where $\boldsymbol{E}$ is the electric field and $(\rho_{\rm b},\boldsymbol{J}_{\rm b})$ and $(\rho_{\rm p},\boldsymbol{J}_{\rm p})$ are the density and current of the beam and plasma, respectively. The plasma density can be expressed as a sum of the electron and ion densities $\rho_{\rm p} = \rho_e + \rho_i$. We will assume a neutral plasma and the ions are stationary such that $\rho_e = \rho_0 + \delta\rho$ and $\rho_i = -\rho_0$, where ρ_0 is the constant background ambient electron plasma density and $\delta\rho$ is the electron plasma density perturbation. By using the Poisson equation $\nabla\cdot\boldsymbol{E} = 4\pi(\rho_{\rm p}+\rho_{\rm b}) = 4\pi(\delta\rho+\rho_{\rm b})$, the linearized fluid momentum equation $4\pi\partial_t\boldsymbol{J}_{\rm p} = \omega_p^2\boldsymbol{E}$, and the continuity equation, the linear electron plasma density perturbation response can be derived and has the form

$$\left(\partial_t^2+\omega_p^2\right)4\pi\delta\rho = -\omega_p^2 4\pi\rho_{\rm b} + \boldsymbol{E}\cdot\nabla\omega_p^2 \ , \tag{10}$$

where $\omega_p^2 = -4\pi e\rho_0/m_e c^2$ is the plasma frequency. Equations (9) and (10) can be Fourier time-decomposed and combined to yield

$$\left(c^2\nabla^2+\omega^2-\omega_p^2\right)\boldsymbol{E} - c^2\nabla\left(\frac{\boldsymbol{E}\cdot\nabla\omega_p^2}{\omega^2-\omega_p^2}\right) = -i4\pi\omega\left[c^2\nabla\left(\frac{\nabla\cdot\boldsymbol{J}_{\rm b}}{\omega^2-\omega_p^2}\right)+\boldsymbol{J}_{\rm b}\right] \ , \tag{11}$$

where we have used the beam density continuity equation $\nabla \cdot \boldsymbol{J}_\mathrm{b} = i\omega\rho_\mathrm{b}$. We will assume that the plasma frequency (ambient background density) is spatially homogeneous such that $\nabla\omega_p^2 = 0$ in the plasma and vacuum regions and the second term on the left-hand side of Eq. (11) vanishes. The wave equation Eq. (11) can then be expressed simply as

$$\left(c^2\nabla^2 + \epsilon\omega^2\right)\boldsymbol{E} = \frac{4\pi}{i\omega\epsilon}\left[c^2\nabla\left(\nabla\cdot\boldsymbol{J}_\mathrm{b}\right) + \omega^2\epsilon\boldsymbol{J}_\mathrm{b}\right] \tag{12}$$

in both the vacuum and plasma regions, where $\epsilon = 1 - \omega_p^2/\omega^2$ is the dielectric constant in the plasma and $\epsilon = 1$ in vacuum. Note that in this analysis we are assuming the absence of external magnetic fields, and we consider a collisionless plasma, which is a good approximation since the collisional frequencies for the parameter regime of interest (e.g., plasma number density $< 10^{18}$ cm^{-3}, electron plasma temperature < 1 keV) are much less than the plasma and radiation frequencies considered.

The transition radiation fields can be calculated by solving the wave equation Eq. (12) in both the vacuum and plasma regions and applying continuity of the normal electric displacement field $\epsilon(\omega)\boldsymbol{E}(\omega)$ and tangential electric field across the boundary [23]. The complete solution to the wave equation Eq. (12) in both the plasma and vacuum regions contains both the particular (particle field) and the homogeneous (radiation field) solutions $\boldsymbol{E} = \boldsymbol{E}_p + \boldsymbol{E}_h$, where the homogeneous solution can be written as $\boldsymbol{E}_h(\omega,\boldsymbol{k}) = \tilde{E}(\omega,\boldsymbol{k})\delta(k^2c^2 - \omega^2\epsilon)$. Note that the homogeneous solution to the wave equation is divergenceless $\boldsymbol{k}\cdot\boldsymbol{E}_h(\omega,\boldsymbol{k}) = 0$. Applying the inverse-Fourier transform of z to the homogeneous solution yields $\boldsymbol{E}_h(\omega,\boldsymbol{k}_\perp,z) = [\tilde{E}/(4\pi ck_z)]\exp(ik_z z)$ with $k_z = \pm(\omega^2\epsilon - c^2k_\perp^2)^{1/2}$ and the $\pm$ indicates waves in the forward (in the vacuum) and backward (in the plasma) going directions with respect to the beam. Substituting the Fourier-transformed beam current [Eq. (8)],

$$\boldsymbol{J}_\mathrm{b}(\omega,\boldsymbol{k}) = -e\sum_{j=1}^{N} c\boldsymbol{\beta}_j 2\pi\delta(\omega - \boldsymbol{k}\cdot\boldsymbol{v}_j)e^{-i\boldsymbol{k}\cdot\boldsymbol{r}_j}\ , \tag{13}$$

into the Fourier-transformed wave equation [Eq. (12)] yields the particular solution

$$\boldsymbol{E}_p(\omega,\boldsymbol{k}) = i4\pi ec^2\sum_{j=1}^{N}\left(\frac{c\boldsymbol{k}}{\omega\epsilon}\boldsymbol{k}\cdot\boldsymbol{\beta}_j - \frac{\omega\boldsymbol{\beta}_j}{c}\right)\frac{2\pi\delta(\omega - \boldsymbol{k}\cdot\boldsymbol{v}_j)}{(c^2k^2 - \epsilon\omega^2)}e^{-i\boldsymbol{k}\cdot\boldsymbol{r}_j}\ . \tag{14}$$

Applying the inverse-Fourier transform of z to the particular solution yields

$$\boldsymbol{E}_p(\omega,\boldsymbol{k}_\perp,z) = i4\pi e\sum_{j=1}^{N}\frac{1}{\beta_{zj}}\frac{(\omega\boldsymbol{\beta}_j - c\boldsymbol{k}/\epsilon)}{(c^2k^2 - \epsilon\omega^2)}\ e^{-i\boldsymbol{k}_\perp\cdot\boldsymbol{r}_{\perp j}}e^{-ik_z(z_j - z)}\big|_{k_z = \omega/v_{zj} - \boldsymbol{k}_\perp\cdot v_{\perp j}/v_{zj}}\ . \tag{15}$$

From the continuity equations across the dielectric interface for the tangential components of the electric field and the normal component of the electric displacement field and using the fact that the homogeneous fields are divergenceless, the radiation fields $\tilde{E}(\omega, \boldsymbol{k}_\perp)$ in both regions ($z < 0$ and $z > 0$) can be solved [23]. In the limit of an ideal conductor-vacuum interface (i.e., assuming $\epsilon \gg 1$ in the plasma and $\epsilon = 1$ in the vacuum), the boundary conditions reduce to $\hat{z} \times [\boldsymbol{E}_h + \boldsymbol{E}_p]_{z=0} = 0$ for the vacuum fields.

The homogeneous electric field in the vacuum $z > 0$ generated by the current traversing the plasma-vacuum boundary can be written as

$$\boldsymbol{E}_h(\omega, \boldsymbol{k}_\perp, z) = -i\frac{4\pi e}{\omega}\sum_{j=1}^{N} \sec\theta \boldsymbol{\mathcal{E}}_j(\boldsymbol{k}_\perp, \boldsymbol{\beta}_j) e^{-i\Psi_j} e^{iz\sqrt{\omega^2/c^2 - k_\perp^2}} \,. \tag{16}$$

where $\Psi_j = \boldsymbol{k}_\perp \cdot \boldsymbol{r}_{\perp j} - (\omega - \boldsymbol{k}_\perp \cdot \boldsymbol{v}_{\perp j}) z_j / v_{zj}$ and $\boldsymbol{\mathcal{E}}_j(\boldsymbol{k}_\perp, \boldsymbol{\beta}_j) = \boldsymbol{\mathcal{E}}_j(\theta, \beta_j, \psi_j, \varphi_j) = \mathcal{E}_{\parallel j}\hat{e}_\parallel + \mathcal{E}_{\perp j}\hat{e}_\perp$. Here $\mathcal{E}_{\parallel j}$ and $\mathcal{E}_{\perp j}$ are the normalized amplitudes of the electric fields generated by an electron in the radiation plane (formed by $\hat{z}$ and $\hat{k}$) and perpendicular to the radiation plane ($\hat{y}$ in the geometry of Fig. 1), respectively. Equation (16) may be decomposed into $\boldsymbol{E}_h = E_\parallel \hat{e}_\parallel + E_\perp \hat{e}_\perp$, with the normal component $\hat{z} \cdot \boldsymbol{E}_h = -E_\parallel \sin\theta$. In the limit of an ideal conductor to vacuum interface (i.e., assuming $|\epsilon| \gg 1$ for $z < 0$ and $\epsilon = 1$ for $z > 0$),

$$\mathcal{E}_{\parallel j}(\theta, u_j, \psi_j, \varphi_j) = \frac{u_j \cos\psi_j \left[u_j \sin\psi_j \cos\varphi_j - \left(1 + u_j^2\right)^{1/2} \sin\theta\right]}{\left[\left(1 + u_j^2\right)^{1/2} - u_j \sin\psi_j \cos\varphi_j \sin\theta\right]^2 - u_j^2 \cos^2\psi_j \cos^2\theta} \,, \tag{17}$$

$$\mathcal{E}_{\perp j}(\theta, u_j, \psi_j, \varphi_j) = \frac{u_j^2 \cos\psi_j \sin\psi_j \sin\varphi_j \cos\theta}{\left[\left(1 + u_j^2\right)^{1/2} - u_j \sin\psi_j \cos\varphi_j \sin\theta\right]^2 - u_j^2 \cos^2\psi_j \cos^2\theta} \,, \tag{18}$$

where $u = p/m_e c = \gamma\beta$ is the normalized momentum of the electrons. Note that, for electrons traversing normal to the dielectric-vacuum boundary, $\mathcal{E}_{\perp j} = 0$ and the transition radiation will be radially polarized. In general, the transition radiation is elliptically polarized. The treatment of the plasma as a perfect metallic conductor is a good approximation for radiation and plasma frequencies such that $|\epsilon| \gtrsim 2$ (see Appendix for further discussion). The transition radiation electric field is the inverse-Fourier transform of Eq. (16),

$$\boldsymbol{E}_h(\boldsymbol{x}, t) = \int \frac{d^2\boldsymbol{k}_\perp}{(2\pi)^2} \int \frac{d\omega}{2\pi} \boldsymbol{E}_h(\omega, \boldsymbol{k}_\perp, z) e^{i\boldsymbol{k}_\perp \cdot \boldsymbol{x}_\perp - i\omega t} \,. \tag{19}$$

B. Radiation energy spectra

The total (integrated over time) energy radiated by the electron beam through a plane in the far-field is given by the integral of the Poynting vector

$$\begin{aligned} dW &= \frac{c}{4\pi}\int_{-\infty}^{\infty} dt \int d^2\boldsymbol{x}_\perp (\boldsymbol{E}\times\boldsymbol{B})\cdot\hat{z} \\ &= \frac{c}{2\pi}\int_{0}^{\infty} \frac{d\omega}{2\pi}\int \frac{d^2\boldsymbol{k}_\perp}{(2\pi)^2}(\hat{k}\cdot\hat{z})\boldsymbol{E}_h^*(\omega,\boldsymbol{k}_\perp,z)\cdot\boldsymbol{E}_h(\omega,\boldsymbol{k}_\perp,z)\ , \end{aligned} \tag{20}$$

where $\boldsymbol{E}_h$ is given by Eq. (16). The energy radiated W per unit frequency $d\omega$ and unit solid angle $d\Omega$ is

$$\begin{aligned} \frac{d^2W}{d\omega d\Omega} &= \frac{\omega^2\cos^2\theta}{(2\pi)^4 c}\boldsymbol{E}_h^*(\omega,\boldsymbol{k}_\perp,z)\cdot\boldsymbol{E}_h(\omega,\boldsymbol{k}_\perp,z) \\ &= \frac{e^2}{\pi^2 c}\sum_{i=1}^{N}\sum_{j=1}^{N}\left(\mathcal{E}_{\parallel i}\mathcal{E}_{\parallel j}+\mathcal{E}_{\perp i}\mathcal{E}_{\perp j}\right)e^{i\Psi_j-i\Psi_i}\ . \end{aligned} \tag{21}$$

The summations over electrons in Eq. (21) may be removed by taking an ensemble average over the six-dimensional electron beam distribution $\tilde{f}(\boldsymbol{r},\boldsymbol{p})$, with the normalization $\int d^3\boldsymbol{r}d^3\boldsymbol{p}\tilde{f}=1$ and momentum distribution given by $g(\boldsymbol{p})=\int d^3\boldsymbol{r}\tilde{f}$. Performing the ensemble average yields

$$\frac{d^2W}{d\omega d\Omega} = \frac{e^2 N}{\pi^2 c}\left\{\int d^3\boldsymbol{p}\left(\mathcal{E}_\parallel^2+\mathcal{E}_\perp^2\right)g(\boldsymbol{p}) + (N-1)\left[\left|\int d^3\boldsymbol{p}g(\boldsymbol{p})\mathcal{E}_\parallel F\right|^2 + \left|\int d^3\boldsymbol{p}g(\boldsymbol{p})\mathcal{E}_\perp F\right|^2\right]\right\}, \tag{22}$$

where F is the spatial form factor defined by

$$F = \frac{1}{g(\boldsymbol{p})}\int d^2\boldsymbol{r}_\perp e^{-i\boldsymbol{k}_\perp\cdot\boldsymbol{r}_\perp}\int dz e^{-iz(\omega-\boldsymbol{k}_\perp\cdot\boldsymbol{v}_\perp)/v_z}\tilde{f}(\boldsymbol{r},\boldsymbol{p})\ . \tag{23}$$

The first term on the right-hand side of Eq. (22) is the contribution from the incoherent radiation ($\propto N$) and the second term on the right-hand side of Eq. (22) is the contribution from the coherent radiation ($\propto N^2$), such that $W = W_{\mathrm{ITR}} + W_{\mathrm{CTR}}$ with

$$\frac{d^2W_{\mathrm{ITR}}}{d\omega d\Omega} = \frac{e^2}{\pi^2 c}N\left[\langle\mathcal{E}_\parallel^2\rangle + \langle\mathcal{E}_\perp^2\rangle\right] \tag{24}$$

$$\frac{d^2W_{\mathrm{CTR}}}{d\omega d\Omega} = \frac{e^2}{\pi^2 c}N(N-1)\left[\left|\langle\mathcal{E}_\parallel F\rangle\right|^2 + \left|\langle\mathcal{E}_\perp F\rangle\right|^2\right] \tag{25}$$

where the brackets indicate an average over the momentum distribution. Note that $\langle\mathcal{E}_\perp\rangle = 0$ for a cylindrically-symmetric momentum distribution.

In the following sections, for simplicity, we will assume no correlations between the position and momentum of the electrons such that the electron beam distribution takes the form $\tilde{f}(\boldsymbol{r},\boldsymbol{p}) = g(\boldsymbol{p})f(\boldsymbol{r})$ and the spatial form factor reduces to

$$F = \int d^2\boldsymbol{r}_\perp e^{-i\boldsymbol{k}_\perp\cdot\boldsymbol{r}_\perp} \int dz e^{-iz(\omega-\boldsymbol{k}_\perp\cdot\boldsymbol{v}_\perp)/v_z} f(\boldsymbol{r}) \; . \tag{26}$$

The spatial form factor Eq. (26) is closely related to the Fourier transform of the electron beam spatial distribution. For a Gaussian spatial beam distribution $f = [(2\pi)^{3/2}\sigma_r^2\sigma_z]^{-1}\exp(-r_\perp^2/2\sigma_r^2)\exp(-z^2/2\sigma_z^2)$, where σ_z and σ_r are the root-mean square (rms) beam duration and radius, respectively, the spatial form factor is $F = F_\perp F_\parallel$, with

$$F_\perp = e^{-\frac{1}{2}(\omega/c)^2\sigma_r^2\sin^2\theta} \; , \tag{27}$$

$$F_\parallel = e^{-\frac{1}{2}[\omega/(c\beta\cos\psi)]^2\sigma_z^2(1-\beta\sin\theta\cos\varphi\sin\psi)^2} \; . \tag{28}$$

For $\psi \ll 1$, i.e., a near collimated beam at the plasma-vacuum boundary, $F_\parallel \simeq \exp[(\omega\sigma_z/v)^2/2]$. As Eqs. (27) and (28) indicate, for radiation wavelengths $\lambda = 2\pi c/\omega$ that are large compared to the dimensions of the beam $\lambda \gg \sigma_r$ and $\lambda \gg \sigma_z$, $F \simeq 1$ and the radiation is fully-coherent. For radiation wavelengths such that $\sigma_r \sin\theta \gg \lambda$ or $\sigma_z \gg \lambda$, the spatial form factor vanishes $F \simeq 0$ and the beam does not radiate coherently $W_{\rm CTR} \simeq 0$.

In deriving the results in this section, it was assumed that the total energy radiated is small compared to the energy stored in the electron beam (as discussed in Sec. II), so that the electron beam distribution remains approximately constant during the radiation process. Also, use of the far-field (or radiation zone) radiation fields requires that the observation position to be sufficiently far from the source, such that the distance from radiator to detector is larger than the radiation formation length $R > L_f$.

C. Self-modulated LWFA electron beam

In this paper, we will assume that the electron beam momentum distribution may be decomposed such that $g(\boldsymbol{p}) = g_\parallel(u)g_\perp(\psi,\varphi)$. The longitudinal momentum distribution of the self-modulated LWFA generated electron bunch can be modeled as a single temperature Boltzmann distribution:

$$g_\parallel(u)du = u_{\rm t}^{-1}\exp\left[-u/u_{\rm t}\right]du \; , \tag{29}$$

where u_t is the temperature of the distribution. Typically, self-modulated LWFA electron bunches will have a temperature of a few MeV (e.g., $u_\mathrm{t} \sim 10$). We will assume the self-modulated LWFA electron bunch transverse momentum distribution can be expressed as a Gaussian distribution $g_\perp(\psi,\varphi)d\psi d\varphi = (\pi\sigma_\perp^2)^{-1}\exp(-\sin^2\psi/\sigma_\perp^2)\sin\psi\cos\psi d\psi d\varphi$. Self-modulated LWFA electron bunches with nC-charge have been demonstrated experimentally [10, 14, 16, 17]. While the electron bunch remains in the plasma, where the background ions provide space charge shielding that prevents blow-up of the dense electron bunches, the bunch duration will typically be on the order of the laser duration ($\sigma_z \lesssim 100$ fs) and the radius on the order of the laser spot size ($\sigma_r \sim 5$ μm).

IV. INCOHERENT TRANSITION RADIATION

In this section we consider the incoherent transition radiation. Using the results of Sec. III B, the energy radiated by a single electron per unit frequency $d\omega$ in solid angle $d\Omega$ is given by $[d^2W_\mathrm{ITR}/d\omega d\Omega]_{e^-} = (e^2/\pi^2 c)(\mathcal{E}_\parallel^2 + \mathcal{E}_\perp^2)$. In the limit of no divergence $\psi = 0$, $\mathcal{E}_\perp = 0$ and the single-electron radiated energy reduces to the well-known result [cf. Eq. (1)]

$$\begin{aligned}\left[\frac{d^2W_\mathrm{ITR}}{d\omega d\Omega}\right]_{e^-} &= \left(\frac{e^2}{\pi^2 c}\right)\frac{u^2\left(1+u^2\right)\sin^2\theta}{\left(1+u^2\sin^2\theta\right)^2} \\ &= \left(\frac{e^2}{\pi^2 c}\right)\frac{\beta^2\sin^2\theta}{\left(1-\beta^2\cos^2\theta\right)^2}\ ,\end{aligned} \tag{30}$$

which can be integrated over solid angle $d\Omega = 2\pi\sin\theta d\theta$ to yield

$$\begin{aligned}\left[\frac{dW_\mathrm{ITR}}{d\omega}\right]_{e^-} &= \left(\frac{2e^2}{\pi c}\right)\left[\frac{\left(1+2u^2\right)}{u\left(1+u^2\right)^{1/2}}\tanh^{-1}\left(\frac{u}{\sqrt{1+u^2}}\right) - 1\right] \\ &= \left(\frac{e^2}{2\pi c\beta}\right)\left[\left(1+\beta^2\right)\ln\left(\frac{1+\beta}{1-\beta}\right) - 2\beta\right]\ .\end{aligned} \tag{31}$$

The total incoherent energy radiated by a beam with N electrons and a normalized momentum distribution $g(\boldsymbol{p})$ is

$$\frac{d^2W_\mathrm{ITR}}{d\omega d\Omega} = N\int d^3\boldsymbol{p}\, g(\boldsymbol{p})\left[\frac{d^2W_\mathrm{ITR}}{d\omega d\Omega}\right]_{e^-}\ . \tag{32}$$

For small electron divergence and observation angles, such that $\psi \ll 1$ and $\theta \ll 1$, the total radiated energy by a cylindrically-symmetric beam distribution is

$$\frac{d^2W_\mathrm{ITR}}{d\omega d\Omega} \simeq \frac{e^2 N}{\pi^2 c}\left[\left(\langle u^2\rangle + \langle u^4\rangle\right)\theta^2 + \langle u^4\rangle\langle\psi^2\rangle\right]\ , \tag{33}$$

where $\langle\psi^2\rangle^{1/2}$ is the rms beam divergence at the plasma-vacuum interface. Note that, for $\theta \ll \psi \ll 1$, $d^2W_{\rm ITR}/d\omega d\Omega \simeq (e^2N/\pi^2c)\langle u^4\rangle\langle\psi^2\rangle$, and the result of finite beam divergence at the plasma-vacuum boundary is to produce incoherent radiation on axis ($\theta = 0$). Without beam divergence, the radiation intensity vanishes on axis. Figure 2 shows the angular distribution of the normalized differential energy spectrum of the incoherent radiation $(\pi^2c/e^2N)d^2W_{\rm ITR}/d\omega d\Omega$ produced by a self-modulated LWFA electron beam ($u_{\rm t} = 10$) assuming a symmetric Gaussian transverse momentum distribution with $\langle\psi^2\rangle^{1/2} = 0$ (dashed line) and $\langle\psi^2\rangle^{1/2} = 0.02$ (solid line).

Equation (33) can be integrated over solid angle, and for a small collection angle $\theta \leq \theta_0 < 1/\langle u\rangle$,

$$\frac{dW_{\rm ITR}}{d\omega} \simeq \frac{e^2N}{2\pi c}\left[\left(\langle u^2\rangle + \langle u^4\rangle\right)\theta_0^4 + 2\langle u^4\rangle\langle\psi^2\rangle\theta_0^2\right] \ . \tag{34}$$

Since the differential incoherent transition radiation spectrum Eq. (24) is frequency independent, the total incoherent energy radiated into a bandwidth $\Delta\omega/\omega$ and small collection angle $\theta \leq \theta_0 < 1/\langle u\rangle$ is

$$W_{\rm ITR} \simeq m_ec^2\frac{r_e}{\lambda}N\frac{\Delta\omega}{\omega}\theta_0^4\left[\left(\langle u^2\rangle + \langle u^4\rangle\right) + 2\langle u^4\rangle\frac{\langle\psi^2\rangle}{\theta_0^2}\right] \tag{35}$$

where $r_e = e^2/m_ec^2 \simeq 2.818\times10^{-15}$ m is the classical electron radius.

V. COHERENT TRANSITION RADIATION

In this section the coherent transition radiation produced at the plasma-vacuum boundary is considered. The energy of the coherent radiation emitted by the electron beam has the form given by Eq. (25). The wavelength dependence is contained in the form factor Eq. (26), which is the Fourier transform of the spatial distribution of the electron beam. Therefore measurement of the energy spectra can provide a method for determining the spatial distribution of the electron beam.

For the case of a collimated beam $g_\perp(\psi) = \delta(\psi)$, $\langle\mathcal{E}_\perp\rangle = 0$, the fields are radially-polarized, and the differential energy spectrum of the coherent transition radiation is

$$\frac{d^2W_{\rm CTR}}{d\omega d\Omega} = \left(\frac{e^2}{\pi^2c}\right)N(N-1)\sin^2\theta\left|\int du g_\parallel(u)F(\omega,\theta,u)\frac{u\left(1+u^2\right)^{1/2}}{1+u^2\sin^2\theta}\right|^2 \ . \tag{36}$$

In general, the differential energy spectrum will be modified by finite beam divergence. For fully-coherent radiation $F \simeq 1$, the energy emitted by a cylindrically-symmetric beam

distribution with small divergence and a small observation angle, such that $u\psi < u\theta < 1$, is

$$\frac{d^2W_{\rm CTR}}{d\omega d\Omega} \simeq \left(\frac{e^2}{\pi^2 c}\right) N(N-1)\theta^2 \left| \int du g_{\parallel} u(1+u^2)^{1/2} \left[1 - \frac{1}{2}\left(1+4u^2\right)\langle\psi^2\rangle\right]\right|^2 , \qquad (37)$$

and for $u > 1$,

$$\frac{d^2W_{\rm CTR}}{d\omega d\Omega} \simeq \left(\frac{e^2}{\pi^2 c}\right) N(N-1)\frac{\theta^2}{4}\left[\left(1+2\langle u^2\rangle\right)^2 - \left(1+2\langle u^2\rangle\right)\left(1+6\langle u^2\rangle + 8\langle u^4\rangle\right)\langle\psi^2\rangle\right] , \quad (38)$$

where $\langle\psi^2\rangle^{1/2}$ is the rms divergence of the electron beam through the plasma-vacuum boundary. For $\theta \ll \psi < 1$, $d^2W_{\rm CTR}/d\omega d\Omega \simeq 0$, and no coherent radiation is observed on axis for a cylindrically-symmetric beam. Physically, this result is due to the fact that the radiation fields produced by the electrons are summed for coherent radiation and the cylindrical symmetry results in the sum vanishing on axis, whereas, in the case of incoherent radiation, the intensities radiated by each electron are summed, resulting in a non-zero incoherent radiation intensity on axis (as shown in Fig. 2). Figure 3 shows the angular distribution of the coherent transition radiation produced by an electron beam with a 5 MeV temperature Boltzmann momentum distribution and a symmetric Gaussian transverse momentum distribution with $\langle\psi^2\rangle^{1/2} = 0$ (dashed line) and $\langle\psi^2\rangle^{1/2} = 0.05$ (solid line). The radiation is assumed to be fully-coherent in Fig. 3. As the figure shows, and indicated by Eq. (38), the effect of beam divergence is to reduce the CTR energy radiated.

Using Eq. (38), the total coherent radiation energy into a small collection angle $\theta \le \theta_0 < 1/\langle u\rangle$, and for a bandwidth $\Delta\omega/\omega$ is

$$W_{\rm CTR} \simeq m_e c^2 \frac{r_e}{\lambda} N(N-1)\frac{\Delta\omega}{\omega}\frac{\theta_0^4}{4}\left[\left(1+2\langle u^2\rangle\right)^2 - \left(1+2\langle u^2\rangle\right)\left(1+6\langle u^2\rangle + 8\langle u^4\rangle\right)\langle\psi^2\rangle\right] . \qquad (39)$$

Equation (39) shows that the coherent transition radiation scales as $W_{\rm CTR} \sim (m_e c^2)(r_e/\lambda)N^2(\Delta\omega/\omega)\theta_0^4\langle u^2\rangle^2$.

VI. EFFECTS OF COHERENT DIFFRACTION RADIATION

The self-field of a relativistic electron extends transversely a distance of the order $\sim \gamma\lambda$. Therefore diffraction radiation from the transverse edge of the plasma-vacuum boundary can be neglected provided $\rho \gg \lambda\gamma$, where ρ is the transverse size of the plasma-vacuum interface. For parameters such that $\rho \sim \lambda\gamma$, diffraction radiation will be produced, limiting

the generation of long-wavelength transition radiation. To estimate the effect of the transverse size of the plasma-vacuum interface, consider the model of a circular dielectric disc (of radius ρ) in the (x, y) plane and an electron beam, with rms radius $\sigma_r \ll \rho$, propagating along the z axis through the dielectric. The resulting radiation will be a combination of transition radiation from the passage of the electron through the dielectric-vacuum interface and diffraction radiation from the transverse edge of the dielectric. The diffraction radiation in the far-field ($R \gg \rho$ and $R \gg \lambda$) may be determined by applying Kirchhoff diffraction theory [7] to the incident fields [i.e., the particle fields, given by Eq. (14)] at the transverse boundary. The electric fields produced by an electron passing through a circular aperture are well-known (for example, Ref. [23]) and, through Babinet's principle [7], may be applied to diffraction from a dielectric disc. For simplicity, in this section we will consider a beam without divergence ($\psi \ll 1$) passing through a ideal circular (radius ρ) conductor ($|\epsilon| \gg 1$).

The differential energy spectrum of the coherent radiation (transition and diffraction) can be expressed as

$$\frac{d^2W_{\rm CR}}{d\omega d\Omega} = \left(\frac{e^2}{\pi^2 c}\right) N(N-1)\sin^2\theta \left| \int du g_{\parallel}(u) F(\omega,\theta,u) \frac{u\,(1+u^2)^{1/2}}{1+u^2\sin^2\theta} D(\omega,\rho,u,\theta) \right|^2 , \quad (40)$$

where $D(\omega, \rho, u, \theta) = D(b, u\sin\theta)$ describes the effect of the diffraction radiation from the transverse boundary:

$$D = 1 - J_0(bu\sin\theta)\left[bK_1(b) + \frac{1}{2}b^2K_0(b)\right] - \frac{1}{2}b^2K_0(b)J_2(bu\sin\theta) , \quad (41)$$

with the parameter $b = k\rho/u$ describing the relative influence of the transverse boundary (i.e., the ratio of the transverse size of the dielectric to the transverse extent of the self-fields of the relativistic electrons). Here J_m and K_m are the $m^{\rm th}$-order regular and modified Bessel functions, respectively. For $b \gg 1$,

$$D \simeq 1 - [J_0(k\rho\sin\theta) + J_2(k\rho\sin\theta)]\sqrt{\frac{b^3\pi}{8}}\exp(-b) , \quad (42)$$

and in the limit of $b \to \infty$, $D = 1$ and Eq. (40) reduces to Eq. (36), i.e., neglecting diffraction radiation is a good approximation in the limit of large transverse dimension $b = k\rho/u \gg 1$. For $b \ll 1$,

$$D \simeq 1 - J_0(k\rho\sin\theta) + \frac{b^2}{2}\left\{ J_0(k\rho\sin\theta) + J_2(k\rho\sin\theta)\left[C_\gamma + \ln\left(\frac{b}{2}\right)\right] \right\} , \quad (43)$$

where C_γ is Euler's constant. In the ultra-relativistic limit, $b \to 0$ and $D = 1 - J_0(k\rho \sin\theta)$.

The radiation generated by a fully-coherent $F \simeq 1$, monoenergetic beam passing through the dielectric ($|\epsilon| \gg 1$) with radius ρ is

$$\frac{d^2W_{\rm CR}}{d\omega d\Omega} = \left(\frac{d^2W_{\rm CTR}}{d\omega d\Omega}\right) D^2(\omega, \rho, u, \theta) \, , \tag{44}$$

where $W_{\rm CTR}$ is given by Eq. (36) for a monoenergetic momentum distribution. The peak of the angular distribution of the coherent radiation from an interface with finite transverse size is shifted compared to the case of a plasma-vacuum boundary with infinite transverse dimension. The peak of the angular distribution of the radiation given by Eq. (44) occurs at $\theta_{\rm peak} \simeq 1/u$ for $b \gg 1$ and $\theta_{\rm peak} \simeq 2.8/(k\rho)$ for $b \ll 1$. The effect of the finite transverse size is that the peak of the angular distribution occurs at a larger angle $\theta_{\rm peak}(b) > 1/u = \theta_{\rm peak}(b \to \infty)$. In the ultra-relativistic limit, $b \ll 1$, and for small observation angles $k\rho \sin\theta \ll 1$, Eq. (44) reduces to $d^2W_{\rm CR}/d\omega d\Omega \simeq (\pi\rho\theta/\lambda)^4 (d^2W_{\rm CTR}/d\omega d\Omega) \ll d^2W_{\rm CTR}/d\omega d\Omega$, which indicates that the total energy radiated is significantly reduced in this regime due to the effects of diffraction radiation.

Figure 4 shows the angular dependence of the differential energy spectrum Eq. (40) produced by an electron beam with a 5 MeV temperature Boltzmann momentum distribution for three cases: $k\rho = 100$ (solid line), $k\rho = 20$ (dotted line), and $k\rho = 5$ (dashed line). As $b = k\rho/u$ decreases, the diffraction radiation strongly modifies the angular distribution [e.g., note the oscillatory behavior characteristic of diffraction radiation evident for $k\rho = 20$ (dotted line)], resulting in the maximum of the differential energy spectrum occurring at larger angles.

As Eq. (40) indicates, the finite transverse extent of the plasma produces a wavelength dependence in the differential energy spectrum for fully-coherent radiation. Figure 5 shows the normalized energy spectrum integrated over solid angle $(dW_{\rm CR}/d\omega)\pi^2 c/e^2 N(N-1)$ radiated by an electron beam with a Boltzmann distribution versus $k\rho = 2\pi\rho/\lambda$ for $u_{\rm t} = 20$ (solid line), $u_{\rm t} = 10$ (dashed line), and $u_{\rm t} = 5$ (dotted line). Figure 5 clearly shows that the spectral content of the radiation is no longer constant, as is the case for ordinary transition radiation from a fully-coherent beam, and that the spectra is strongly modified by the diffraction radiation for parameters $b \sim 1$ (i.e., $\lambda \sim \rho/\gamma$). Distortion of the spectra increases with larger energy, and for decreasing transverse size, the spectra is suppressed. For large transverse size ($b \gg 1$), the fully-coherent spectra becomes constant (i.e., the limit

of transition radiation from an infinite transverse boundary). In general, the spectral region of coherent radiation is approximately $2\pi\sigma_z < \lambda < 2\pi\rho/u$, where the lower bound is due to longitudinal coherence [F in Eq. (40)], and the upper bound is due to diffraction radiation effects [D in Eq. (40)].

VII. COHERENT THZ RADIATION FROM A SELF-MODULATED LWFA ELECTRON BEAM

Recent self-modulated LWFA experiments have produced relativistic electrons with longitudinal momentum distributions given by Eq. (29) with temperatures typically a few MeV [10]. In such experiments, an intense laser pulse is focused into a gas jet with dimensions $\lesssim 1$ mm. The laser pulse ionizes the gas and becomes self-modulated through Raman scattering, generating a high phase velocity plasma wave. Background plasma electrons can become trapped by heating (through the interaction with the backward scattered light) or by wavebreaking (where the plasma wave drives fluid oscillations with velocities near the plasma wave phase velocity). These trapped electrons are then accelerated by the plasma wave. The self-modulated LWFA can produce nC electron bunches of duration on the order of the laser duration ($\sigma_z/c \lesssim 100$ fs) and radius on the order of the laser spot size ($\sigma_r \sim 5$ μm). When the electron bunch exits the plasma, radiation is emitted from the interaction with the plasma-vacuum boundary.

The interaction of these extremely dense laser-plasma-generated electron bunches with the plasma-vacuum boundary can produce coherent radiation for wavelengths longer than the bunch dimensions. For example, Eq. (36) predicts that the total energy radiated by a 2 nC laser-plasma-generated electron bunch, with a 5 MeV temperature Boltzmann distribution, in the spectral range $\lambda = 0.1$–1 mm and within the collection angle $\theta \leq 100$ mrad, is $W = 98$ μJ. This energy per pulse is several orders of magnitude beyond current state-of-the-art THz sources [6, 8].

For the laser-plasma acceleration experiments, the transverse plasma boundary is typically $\rho \lesssim 1$ mm. Therefore coherent THz radiation will be strongly modified by the diffraction radiation produced by the finite transverse size of the plasma. Equation (40) can be solved for the case of a self-modulated LWFA-generated electron bunch distribution. Figure 6 shows the dependence of total coherent energy radiated in the spectral range $\lambda =$

0.1–1 mm normalized to the charge $W[\mathrm{nJ}]/(Q[\mathrm{nC}])^2$, generated by a 5 MeV temperature self-modulated LWFA generated electron bunch versus transverse plasma radius ρ, within a collection angle of $\theta \leq 50$ mrad, $\theta \leq 100$ mrad, and $\theta \leq 200$ mrad. Figure 6 shows that, for this spectral range, the energy radiated can be increased several orders of magnitude by increasing the transverse size of the plasma, and this source (e.g., a ~ 1 nC, ~ 5 MeV temperature self-modulated LWFA-generated electron bunch) has the capability to produce THz radiation with a flux of 100 μJ/pulse.

VIII. SUMMARY AND CONCLUSIONS

A general theory of transition radiation has been presented that describes both the incoherent and coherent radiation emitted by an electron bunch traversing a plasma-vacuum boundary. By using the dense, short electron bunches produced by a LWFA, unprecedented levels of CTR can be generated at the plasma-vacuum boundary where the bunch is still ultrashort and extremely dense, i.e., before the electron bunch undergoes space charge blow-up in vacuum. Coherent emission requires that the longitudinal and transverse form factors be near unity, e.g., for wavelengths long compared to the bunch dimensions. To accurately model experiments in the self-modulated LWFA regime, the effects of the longitudinal and transverse momentum distributions were examined for both the ITR and CTR. It was shown that finite beam divergence produces on-axis radiation for ITR. For CTR from a cylindrically-symmetric beam with finite divergence, the angular distribution of radiated energy is zero on axis and the total energy radiated is reduced.

In the limit of a semi-infinite plasma, the CTR energy radiated in a narrow bandwidth $\Delta\omega$ within a cone angle θ_0 scales as $W \propto N^2(u_\mathrm{t}\theta_0)^4$. Hence, the CTR energy can be increased by increasing the bunch charge (N), the opening angle of the collection optics (θ_0), and the electron energy (u_t). The analysis in this paper indicates that for parameters obtainable in present day experiments, self-modulated LWFA generated electron bunches have the capability of producing intense THz radiation, of order 100 μJ/pulse at the plasma-vacuum interface, several orders of magnitude beyond current state-of-the-art THz sources.

One factor limiting the CTR energy is the small transverse size of the plasma. This is of concern since the plasmas used in the self-modulated LWFA are typically produced via tunneling ionization from the pump laser pulse and have a transverse dimension $\lesssim 1$ mm.

To model the finite transverse extent of the plasma, the effect of the diffraction radiation was included in the analysis. The finite transverse extent of the plasma was shown to significantly reduce the long-wavelength transition radiation $\lambda > \rho/\gamma$. This restriction can be overcome in a straightforward manner by using additional laser pulses to pre-ionize a larger region of plasma. Also assumed in the analysis was a sharp transition between the plasma and vacuum. However, for sufficiently short wavelength radiation the scale length of the plasma-vacuum boundary will be comparable to the radiation formation length, and this assumption will no longer be valid.

This paper has focused on the production of CTR from LWFAs, i.e., intense laser pulses interacting with gas jets (underdense plasmas). Transition radiation will also occur from intense laser pulses interacting with solid targets (overdense plasmas) [34]. For example, when an intense laser pulse strikes the front surface of a foil, energetic electron are generated near the front surface through a combination of ponderomotive and parametric processes. This results in a beam of relativistic electrons, which for sufficiently thin foils, can generate CTR as the beam emerges from the rear side of the target.

In addition to being an intense source of THz and far infrared radiation, this radiation can also be used as a diagnostic for the electron bunch structure, due to the correlation between the bunch dimensions and the rapid fall off of the CTR signal for short wavelengths. Although a direct measurement of the the longitudinal bunch structure has not been made in a LWFA, theory and simulation indicate that the bunch length should be on the order of the laser pulse length ($\gtrsim$ 50 fs). In the self-modulated regime, simulations indicate that the electron bunch may be sub-bunched at the plasma wavelength, which is on the order of 10 μm for a plasma density of 10^{19} cm^{-3}, as used in present day experiments. Furthermore, future experiments may test such novel concepts as the colliding laser pulse injection [35, 36], simulations of which predict electron bunch durations on the order of 10 fs (a few microns). The fine longitudinal structure that may be present on a electron bunch in the self-modulated regime, or the extremely short bunches predicted for a colliding pulse injector, imply that such bunches can generate CTR in unprecedented short wavelength regimes, i.e., from a few to tens of microns. For increasing bunch charge and decreasing bunch length, it is possible that the total energy radiated by CTR approaches the total kinetic energy of the electron bunch, particularly for modest energy electron bunches. This could significantly alter the electron energy distribution of the self-modulated LWFA electron bunch as it exits

the plasma (particularly for the low energy component of the distribution). In this limit, an accurate analysis of CTR and the electron beam distribution must include the self-consistent energy loss of the electrons due to the radiation process.

APPENDIX: FINITE PLASMA DIELECTRIC CONSTANT

In this Appendix we consider the influence of a finite plasma dielectric and show that the plasma-vacuum interface can be well-modeled by a conductor-vacuum interface provided $\omega_p > \omega$. Consider a single electron normal to the plasma-vacuum interface. For a single electron normal to the plasma-vacuum interface, the energy of the transition radiation emitted into the vacuum for arbitrary dielectric constant ϵ, in frequency range $d\omega$ and solid angle $d\Omega$, is given by [23]

$$\frac{d^2W_e}{d\omega d\Omega} = \frac{e^2}{\pi^2 c}\frac{\beta^2 \sin^2\theta\cos^2\theta}{\left(1-\beta^2\cos^2\theta\right)^2}\left|\frac{(\epsilon-1)\left[1-\beta^2-\beta\left(\epsilon-\sin^2\theta\right)^{1/2}\right]}{\left[\epsilon\cos\theta+\left(\epsilon-\sin^2\theta\right)^{1/2}\right]\left[1-\beta\left(\epsilon-\sin^2\theta\right)^{1/2}\right]}\right|^2 . \quad \text{(A.1)}$$

In the long radiation wavelength, high plasma density limit $\epsilon = 1-\omega_p^2/\omega^2 \to -\infty$, Eq. (A.1) reduces to Eq. (30). For $|\epsilon|\cos\theta \gg 1$ and $|\epsilon|\beta \gg 1$, Eq. (A.1) reduces to

$$\frac{d^2W_e}{d\omega d\Omega} \simeq \frac{e^2}{\pi^2 c}\frac{\beta^2\sin^2\theta}{\left(1-\beta^2\cos^2\theta\right)^2}\left[1+\frac{\left(\beta\cos\theta-1\right)^2}{|\epsilon|\cos^2\theta}\right] , \quad \text{(A.2)}$$

or, with $\gamma \gg 1$ and $\theta \ll 1$,

$$\frac{d^2W_e}{d\omega d\Omega} \simeq \frac{e^2}{\pi^2 c}\frac{\theta^2}{\left(\theta^2+\gamma^{-2}\right)^2}\left[1+\left(\theta^2+\gamma^{-2}\right)^2|\epsilon|^{-1}\right] . \quad \text{(A.3)}$$

Equation (A.3) indicates that even for a relatively small plasma dielectric constant, i.e., $|\epsilon| \gtrsim 1$, the plasma can be well-approximated by a conductor. Figure 7 shows the energy spectra $dW_e/d\omega$ calculated from Eq. (A.1), normalized to the infinite-dielectric constant result calculated from Eq. (30), versus dielectric constant $\epsilon = 1-\omega_p^2/\omega^2$, emitted within $\theta \leq$ 200 mrad, by an electron with $\gamma = 20$ (solid curve), 10 (dashed curve), and 5 (dotted curve). Figure 7 indicates that modeling the plasma as a conductor is a good approximation (i.e., within a few percent) for long wavelength radiation $\omega < \omega_p$.

ACKNOWLEDGMENTS

This work was supported by the U.S. Department of Energy under Contract No. DE-AC03-76SF0098.

[1] D. M. Mittleman, M. Gupta, R. Neelamani, R. G. Baraniuk, J. V. Rudd, and M. Koch, Appl. Phys. B **68**, 1085 (1999).

[2] J. Orenstein and A. J. Millis, Science **288**, 468 (2000).

[3] B. Ferguson, S. Wang, D. Gray, D. Abbot, and X.-C. Zhang, Opt. Lett. **27**, 1312 (2002).

[4] A. S. Weling, B. B. Hu, N. M. Froberg, and D. H. Auston, Appl. Phys. Lett. **64**, 137 (1994).

[5] X.-C. Zhang, B. B. Hu, J. T. Darrow, and D. H. Auston, Appl. Phys. Lett. **56**, 1011 (1990).

[6] E. Budiarto, J. Margolies, S. Jeong, J. Son, and J. Bokor, IEEE J. Quantum Electron. **32**, 1839 (1996).

[7] J. D. Jackson, *Classical Electrodynamics* (Wiley, New York, 1975).

[8] G. L. Carr, M. C. Martin, W. R. McKinney, K. Jordan, G. Neil, and G. P. Williams, Nature **420**, 153 (2002).

[9] W. P. Leemans, C. G. R. Geddes, J. Faure, C. Tóth, J. van Tilborg, C. B. Schroeder, E. Esarey, G. Fubiani, D. Auerbach, B. Marcelis, et al., Phys. Rev. Lett. (2003), submitted for publication.

[10] W. P. Leemans, P. Catravas, E. Esarey, C. G. R. Geddes, C. Toth, R. Trines, C. B. Schroeder, B. A. Shadwick, J. van Tilborg, and J. Faure, Phys. Rev. Lett. **89**, 174802 (2002).

[11] E. Esarey, P. Sprangle, J. Krall, and A. Ting, IEEE Trans. Plasma Sci. **24**, 252 (1996).

[12] A. Modena, Z. Najmudin, A. E. Dangor, C. E. Clayton, K. A. Marsh, C. Joshi, V. Malka, C. B. Darrow, C. Danson, D. Neely, et al., Nature **377**, 606 (1995).

[13] A. Ting, C. I. Moore, K. Krushelnick, C. Manka, E. Esarey, P. Sprangle, R. Hubbard, H. R. Burris, R. Fischer, and M. Baine, Phys. Plasmas **4**, 1889 (1997).

[14] C. Gahn, G. D. Tsakiris, A. Pukhov, J. Meyer-ter-Vehn, G. Pretzler, P. Thirolf, D. Habs, and K. J. Witte, Phys. Rev. Lett. **83**, 4772 (1999).

[15] X. Wang, M. Krishnan, N. Saleh, H. Wang, and D. Umstadter, Phys. Rev. Lett. **84**, 5324 (2000).

[16] V. Malka, J. Faure, J. R. Marquès, F. Amiranoff, J. P. Rousseau, S. Ranc, J. P. Chambaret, Z. Najmudin, B. Walton, P. Mora, et al., Phys. Plasmas **8**, 2605 (2001).

[17] M. I. K. Santala, Z. Najmudin, E. L. Clark, M. Tatarakis, K. Krushelnick, A. E. Dangor, V. Malka, J. Faure, R. Allott, and R. J. Clarke, Phys. Rev. Lett. **86**, 1227 (2001).

[18] C. D. Decker, W. B. Mori, and T. Katsouleas, Phys. Rev. E **50**, R3338 (1994).

[19] K.-C. Tzeng, W. B. Mori, and T. Katsouleas, Phys. Rev. Lett. **79**, 5258 (1997).

[20] A. Pukhov, Z.-M. Sheng, and J. Meyer-ter-Vehn, Phys. Plasmas **6**, 2847 (1999).

[21] G. Fubiani, G. Dugan, W. Leemans, E. Esarey, and J. L. Bobin, in *Proceedings of the 2002 Advanced Accelerator Concepts Workshop*, edited by C. E. Clayton and P. Muggli (Amer. Inst. Phys., New York, 2002), vol. 647, pp. 203–212.

[22] V. L. Ginzburg and I. M. Frank, JETP **16**, 15 (1946).

[23] M. L. Ter-Mikaelian, *High-energy electromagnetic processes in condensed media* (Wiley-Interscience, New York, 1972).

[24] U. Happek, A. J. Sievers, and E. B. Blum, Phys. Rev. Lett. **67**, 2962 (1991).

[25] Y. Shibata, T. Takahashi, T. Kanai, K. Ishi, M. Ikezawa, J. Ohkuma, S. Okuda, and T. Okada, Phys. Rev. E **50**, 1479 (1994).

[26] P. Kung, H.-C. Lihn, H. Wiedemann, and D. Bocek, Phys. Rev. Lett. **73**, 967 (1994).

[27] G. P. Le Sage, T. E. Cowan, R. B. Fiorito, and D. W. Rule, Phys. Rev. ST Accel. Beams **2**, 122802 (1999).

[28] K. N. Ricci and T. I. Smith, Phys. Rev. ST Accel. Beams **3**, 032801 (2000).

[29] J. Zheng, K. A. Tanaka, T. Miyakoshi, Y. Kitagawa, R. Kodama, T. Kurahashi, and T. Yamanaka, Phys. Plasmas **9**, 3610 (2002).

[30] Y. Shibata, S. Hasebe, K. Ishi, T. Takahashi, T. Ohsaka, M. Ikezawa, T. Nakazato, M. Oyamada, S. Urasawa, T. Yamakawa, et al., Phys. Rev. E **52**, 6787 (1995).

[31] A. W. Chao and M. Tigner, eds., *Handbook of accelerator physics and engineering* (World Scientific, Singapore, 1999).

[32] W. P. Leemans, D. Rodgers, P. E. Catravas, C. G. R. Geddes, G. Fubiani, E. Esarey, B. A. Shadwick, R. Donahue, and A. Smith, Phys. Plasmas **8**, 2510 (2001).

[33] J. V. Lepore and R. J. Riddell, Jr., Phys. Rev. D **13**, 2300 (1976).

[34] J. J. Santos, F. Amiranoff, S. D. Baton, L. Gremillet, M. Koenig, E. Martinolli, M. Rabec Le Gloahec, C. Rousseaux, D. Batani, A. Bernardinello, et al., Phys. Rev. Lett. **89**, 025001 (2002).

[35] E. Esarey, R. F. Hubbard, W. P. Leemans, A. Ting, and P. Sprangle, Phys. Rev. Lett. **79**, 2682 (1997).

[36] C. B. Schroeder, P. B. Lee, J. S. Wurtele, E. Esarey, and W. P. Leemans, Phys. Rev. E **59**,

6037 (1999).

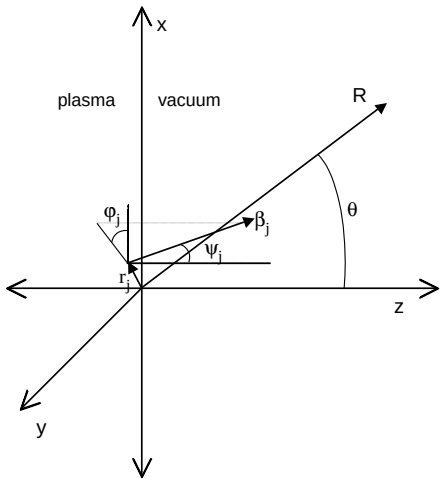

FIG. 1: Geometry of calculation: r_j is the position of the $j^{\rm th}$ particle at $z = 0$ [in the (x, y) plane], ψ_j is the angle of the electron velocity $\boldsymbol{\beta}_j$ with respect to the z axis, φ_j is the angle of the transverse projection of $\boldsymbol{\beta}_j$ with respect to the x axis, and θ is the angle the observation vector $\boldsymbol{R}$ makes with the z axis.

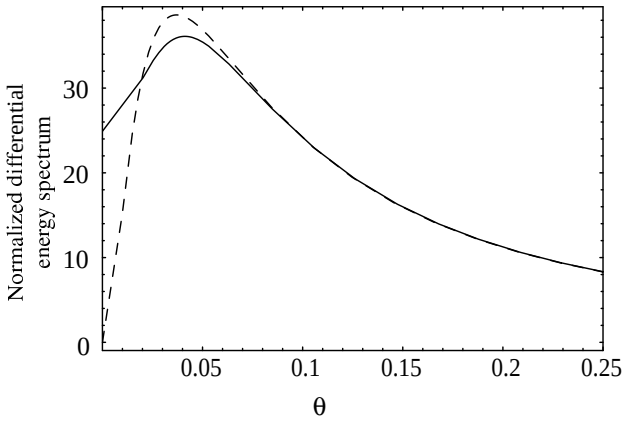

FIG. 2: Normalized differential energy spectrum for the incoherent radiation $(\pi^2 c/e^2 N) d^2 W_{\rm ITR}/d\omega d\Omega$ versus observation angle θ generated by an electron beam with a 5 MeV temperature Boltzmann momentum distribution and a Gaussian transverse momentum distribution with $\langle \psi^2 \rangle^{1/2} = 0$ (dashed line) and $\langle \psi^2 \rangle^{1/2} = 0.02$ (solid line).

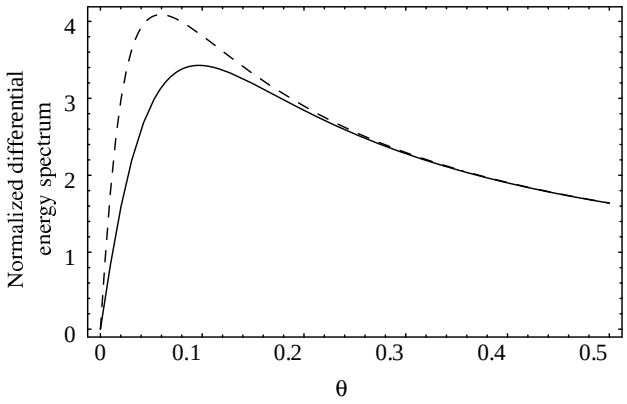

FIG. 3: Normalized differential energy spectrum for the coherent radiation $[\pi^2 c/e^2 N(N-1)]d^2W_{\rm CTR}/d\omega d\Omega$ versus observation angle θ generated by an electron beam with a 5 MeV temperature Boltzmann momentum distribution and a Gaussian transverse momentum distribution with $\langle\psi^2\rangle^{1/2} = 0$ (dashed line) and $\langle\psi^2\rangle^{1/2} = 0.05$ (solid line).

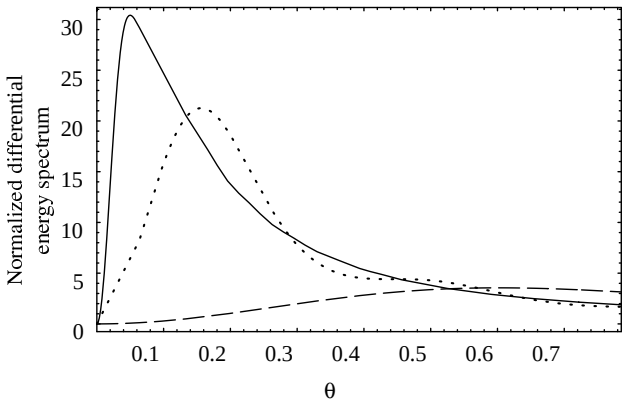

FIG. 4: Angular distribution of normalized differential energy spectrum for the fully-coherent radiation (transition and diffraction) $[\pi^2 c/e^2 N(N-1)]d^2W_{\rm CR}/d\omega d\Omega$ generated by an electron beam with a 5 MeV temperature Boltzmann momentum distribution with $k\rho = 100$ (solid line), $k\rho = 20$ (dotted line), and $k\rho = 5$ (dashed line).

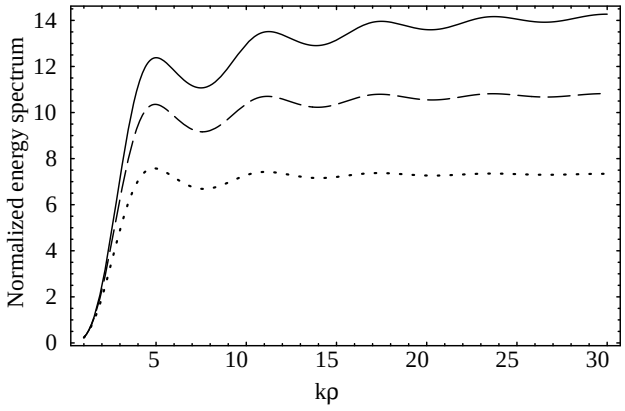

FIG. 5: Normalized energy spectrum integrated over solid angle $[\pi^2 c/e^2 N(N-1)]dW_{\rm CR}/d\omega$ radiated by an electron beam with a Boltzmann distribution versus $k\rho = 2\pi\rho/\lambda$ for $u_{\rm t} = 20$ (solid line), $u_{\rm t} = 10$ (dashed line), and $u_{\rm t} = 5$ (dotted line).

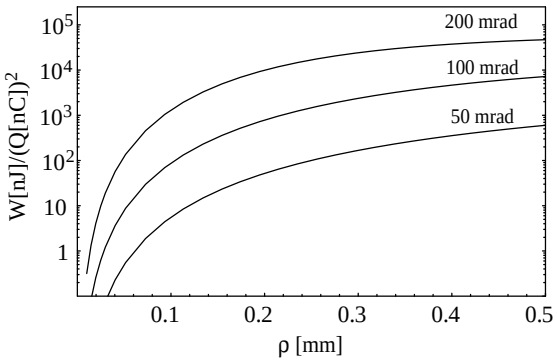

FIG. 6: Total coherent energy radiated in the spectral range $\lambda = 0.1$–1 mm normalized to the charge $W[\mathrm{nJ}]/(Q[\mathrm{nC}])^2$, generated by 5 MeV temperature self-modulated LWFA-generated electron bunch versus transverse plasma radius ρ within the collection angles: $\theta \leq 50$ mrad, $\theta \leq 100$ mrad, and $\theta \leq 200$ mrad.

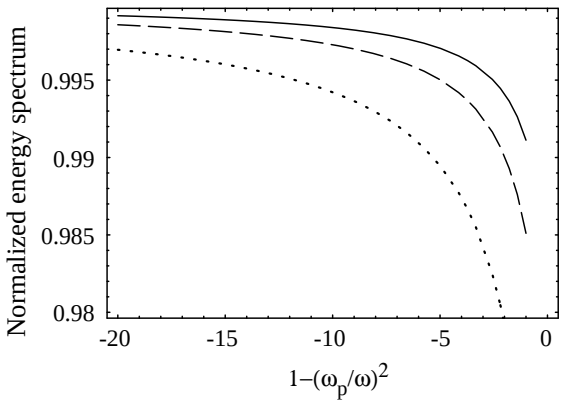

FIG. 7: Energy spectra $dW_e/d\omega$ emitted by a single electron traversing normal to the plasma-vacuum interface [cf. Eq. (A.1)] normalized to the conductor-vacuum result [cf. Eq. (30)] versus dielectric constant $\epsilon = 1 - \omega_p^2/\omega^2$, emitted within $\theta \leq 200$ mrad, with $\gamma = 20$ (solid curve), 10 (dashed curve), and 5 (dotted curve).